

# Raster2Seq: Polygon Sequence Generation for Floorplan Reconstruction

Hao Phung      Hadar Averbuch-Elor  
 Cornell University

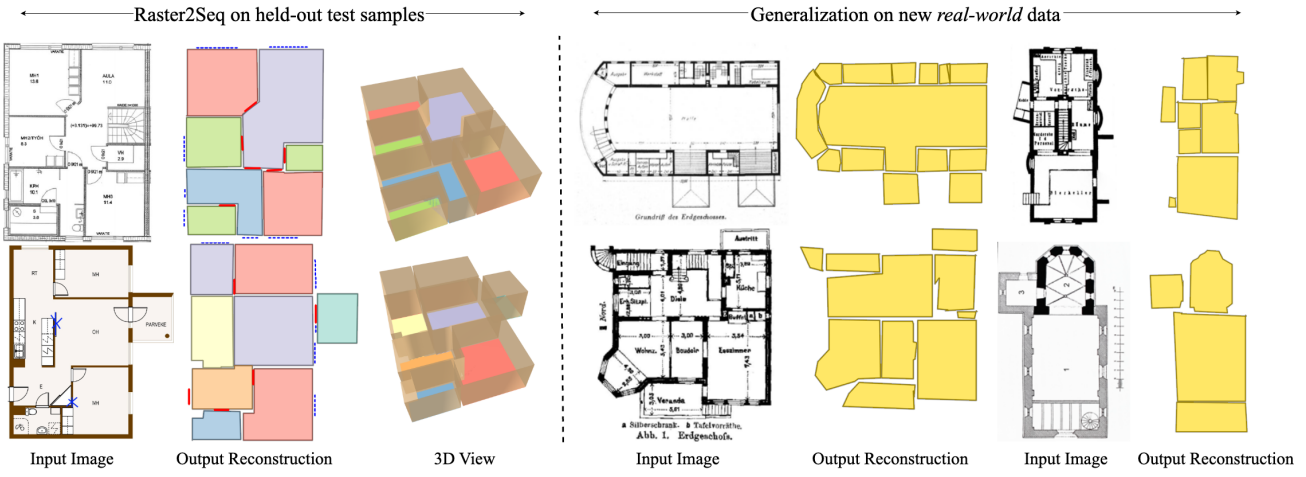


Figure 1. Our approach transforms rasterized floorplan images to vectorized format, reconstructing both its structure and semantics. We illustrate\* results on held-out CubiCasa5K [17] test samples (left). The colors denote unique semantic categories (e.g., `Outdoor`, `Bedroom`, `bath`, and `entry`). Additionally, we highlight our model’s generalization capabilities over complicated real-world floorplan images from WAFFLE [13] (right). \*3D visualizations are constructed by extending the 2D boundaries vertically.

## Abstract

Reconstructing a structured vector-graphics representation from a rasterized floorplan image is typically an important prerequisite for computational tasks involving floorplans such as automated understanding or CAD workflows. However, existing techniques struggle in faithfully generating the structure and semantics conveyed by complex floorplans that depict large indoor spaces with many rooms and a varying numbers of polygon corners. To this end, we propose Raster2Seq, framing floorplan reconstruction as a sequence-to-sequence task in which floorplan elements—such as rooms, windows, and doors—are represented as labeled polygon sequences that jointly encode geometry and semantics. Our approach introduces an autoregressive decoder that learns to predict the next corner conditioned on image features and previously generated corners using guidance from learnable anchors. These anchors represent spatial coordinates in image space, hence allowing for effectively directing the attention mechanism to focus on informative image regions. By embracing the autoregressive mechanism, our method offers flexibility in the output format, enabling for efficiently handling complex floorplans with numerous rooms and diverse polygon structures. Our method achieves state-of-the-art performance on standard benchmarks such as Structure3D, CubiCasa5K, and Raster2Graph, while also demonstrating strong generalization to more challenging datasets like WAFFLE, which contain diverse room structures and complex geometric variations.

## 1. Introduction

Floorplans are a fundamental element of architectural design that define the structure and semantics of indoor spaces, from the tiny studio apartment in Manhattan to the historic Café Helms in Berlin (depicted in the top right corner of Figure 1). While floorplans are typically drawn in a vector-graphics representation using specialized softwares (e.g., AutoCAD),

they are usually distributed in rasterized image formats. This rasterization process strips away the structured geometric and semantic information, severely limiting their utility for computational tasks such as automated editing [32, 36, 49], floorplan understanding [30, 42], or 3D reconstruction [22, 28, 31].

To unlock computational capabilities over rasterized floor-

plans, several works have explored the *raster-to-vector* conversion task [11, 23, 48], which aims to transform an input floorplan image back to vectorized format. However, despite the significant advancements enabled by Transformer-based architectures [6, 16, 47], existing methods face challenges in capturing the structure and semantics conveyed by complicated real-world floorplans, often depending on pretrained detectors and constructing sub-optimal multi-stage pipelines for performing the conversion.

In this work, we propose *Raster2Seq*, an approach that transforms rasterized floorplan images to vectorized format using a labeled polygon sequence representation. Unlike prior work that simultaneously predict all structural floorplan elements [6, 37, 47], our framework autoregressively outputs a polygon sequence, directly modeling both spatial structure and semantic attributes. Our key observation, motivating our framework design, is that floorplan elements can be effectively modeled as a sequence, leveraging the left-to-right generation bias of masked attention models [40]. This allows us to decompose floorplan reconstruction into interpretable, sequential predictions mirroring the natural CAD design workflow. We represent each polygon as a sequence of labeled corners, *i.e.*, spatial coordinates labeled with semantic information, and sort the floorplan’s polygons using a left-to-right ordering. Specifically, we consider rooms, windows and doors, but this representation could easily accommodate additional labeled entities. At its core, our framework introduces an anchor-based autoregressive decoder that effectively fuses information from image features and the previously generated corners to predict the next labeled corner. In particular, our autoregressive module is guided by learnable anchors that direct the attention mechanism to focus on informative regions, enabling for efficiently handling complex floorplan images. We achieve this without sacrificing semantic fidelity by additionally introducing a token-level semantic classification loss that supervises semantic information over individual corner embeddings.

We show the effectiveness of our framework on multiple benchmarks, conducting experiments in different floorplan reconstruction settings—considering both rasterized RGB images and 2D density maps as input. Our approach consistently surpasses existing methods over a wide range of geometric and semantic metrics. Notably, our results show that more complicated floorplans—containing higher quantities of corners and rooms—yield larger performance gaps. We also show strong generalization capabilities over challenging real-world Internet datasets, demonstrated both qualitatively and quantitatively. Code and models will be available.

## 2. Related Work

### 2.1. Floorplan Reconstruction

Raster-to-vector floorplan conversion aims to reconstruct vectorized representations from rasterized floorplan images.

Prior to deep learning, multi-step systems [2, 11, 27] relied on handcrafted features to detect floorplan components (e.g. walls). Liu *et al.* [23] first integrated neural networks for solving this task, predicting corner representations followed by integer programming to recover geometric primitives. Subsequent works utilized pixel-wise segmentation [48] and graph neural networks [38] to model hierarchical relationships among floorplan elements. Raster2Graph [16] employs a transformer [51] with image-space augmentation to highlight visible corners for sequential corner prediction. By contrast, our method formulates floorplan conversion as a sequence-to-sequence task, generating polygon coordinates autoregressively. This naturally handles variable-length polygons and dense layouts without requiring image augmentation or corner sampling strategies.

Several works address related floorplan reconstruction tasks using different modalities such as point-cloud density maps [6, 37, 47] and RGB panoramas [4, 24], rather than rasterized floorplan images. Early methods like Floor-SP [5] and MonteFloor [37] frame the task as instance segmentation with additional optimization steps, but these multi-stage pipelines typically generalize poorly to diverse floorplan layouts. More recent end-to-end approaches eliminate post-optimization: HEAT [6] and FRI-Net [44] follow bottom-up strategies—detecting corners then classifying edges, or predicting line primitives then grouping them into rooms. RoomFormer [47] and PolyRoom [26] formulate floorplan reconstruction as object detection, predicting room coordinates through numerous object queries (e.g., 2800) with Hungarian matching. While these methods were originally designed for 3D-scan-based inputs, we demonstrate that they can be adapted for raster-to-vector conversion. However, as demonstrated in our experiments, when floorplan complexity exceeds this fixed query capacity, performance degrades significantly. Moreover, these methods cannot output a number of predictions beyond a predefined number of corners and rooms per image. By contrast, our method is not limited by a fixed number of predictions, generating ordered, non-redundant outputs sequentially, without additional post-processing steps for extracting semantic predictions.

**Semantic integration.** Unlike most prior work that focuses solely on structural prediction, our method also incorporates semantic information. RoomFormer and Raster2Graph also integrate semantics. However, RoomFormer loses fine-grained semantic information by averaging corner embeddings within uniform-length room sequences—inevitably including padding corners—before classification. Raster2Graph introduces unnecessary complexity by predicting four neighbor room classes per corner, causing potential error propagation and additional computational overhead. In contrast, our approach employs granular token-level supervision, where each corner receives direct gradient updates without dilution from padding. Since rooms are

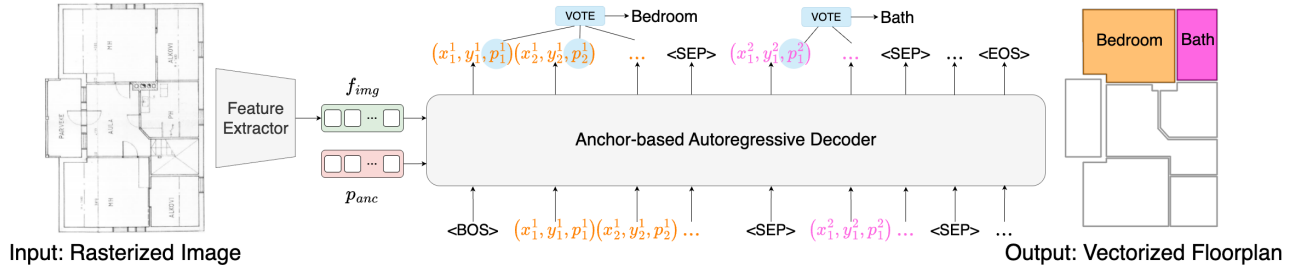


Figure 2. **Method Overview.** Given a rasterized floorplan image (left), our approach converts it into vectorized format, represented as a labeled polygon sequence, separated using special  $<\text{SEP}>$  tokens. The main architectural component of our framework is an anchor-based autoregressive decoder, which predicts the next token given image features ( $f_{img}$ ), learnable anchors ( $v_{anc}$ ) and the previously generated tokens; see Section 3.2 for additional details. Above, we visualize the first two labeled polygons predicted (colored in orange and pink, respectively).

inherently variable-length polygons, our token-level loss naturally aligns with this representation.

## 2.2. Sequence-to-Sequence Modeling for Visual Tasks

Sequence-to-sequence (seq2seq) modeling [39] was originally proposed for machine translation, with the goal of learning a mapping from a source sequence to a target sequence. This framework was later adapted to a plethora of computer vision tasks by providing image features as input to a decoder (typically an RNN or Transformer) that generates a target sequence. Notable applications include image captioning [10, 41, 45], object detection [8], instance segmentation [1, 9, 25], and image generation [35, 46]. The seq2seq paradigm enables end-to-end training and naturally accommodates inputs and outputs of variable lengths, eliminating the need for complex post-processing. This paradigm was adopted by Liu *et al.* [25] for representing object segmentations as polygon sequences, which can be utilized for the task of prompt-based segmentation. While our method is conceptually similar, our framework introduces several representation and architectural differences for performing floorplan reconstruction. For example, beyond predicting spatial coordinates, we introduce semantic labels into the representation and incorporate a novel semantic training objective for semantic-aware floorplan recognition. This semantic integration improves the utility of vectorized floorplans by producing both structural information and semantic labels.

Prior work has explored the effectiveness of recursive frameworks in modeling complex and structured visual data. For instance, GRASS [19] GRAINS [20], READ [33], SceneScript [3] demonstrated the utility of recursive prediction for 3D shapes, 3D indoor scene synthesis, 2D document layout generation, and 3D scene reconstruction, respectively. More closely related to our work, SceneScript formulates 3D scenes as text representations and learns to generate house layouts from input point clouds using predefined text com-

mands for drawing objects (e.g. wall and object box). In our work, we adopt the sequence-to-sequence framework for floorplan transformation, predicting semantic polygon coordinates sequentially based on corner-based representation instead.

## 3. Method

An overview of our proposed method is presented in Figure 2. Our goal is to transform a rasterized floorplan image into vectorized format, reconstructing both its structure and semantics. Specifically, we assume that we are provided with an RGB image of a rasterized floorplan  $I \in \mathbb{R}^{H \times W \times 3}$ , where  $H$  and  $W$  denote the height and width of the image. The input image  $I$  is encoded via a *Feature Extractor* module to produce a feature vector  $f_{img} \in \mathbb{R}^{L_I \times D}$  where  $L_I$  is the length of the image features and  $D$  is the number of channels.

Unlike existing floorplan reconstruction techniques [6, 37, 38, 48] that extract vectorized floorplans via intermediate geometric elements such as edges, corners, or room segments, we propose to represent vectorized floorplans directly using a sequence of labeled polygons. We introduce this representation in Section 3.1. We then describe our *Anchor-based Autoregressive Decoder* module, the main architectural component in our framework, in Section 3.2. Finally, training and inference details are discussed in Section 3.3.

### 3.1. Labeled Polygon Sequence Floorplan Representation

We propose to represent vectorized floorplans using labeled polygon sequences. By labeled, we refer to the polygon’s *semantics*. For instance, a room can be labeled as a *kitchen*, *bedroom*, etc. We parameterize a polygon as a sequence of labeled corner tokens  $c$ , where  $c_i = (x_i, y_i, p_i)$  denotes the  $i$ -th corner in the polygon,  $v_i = (x_i, y_i)$  denotes its spatial position, and  $p_i \in [0, 1]^C$  denotes its semantic probability vector (assuming  $C$  unique semantic categories). As we elaborate later in Section 3.3, room-level semantic predic-

tions are obtained by aggregating semantic information at the token-level. We also consider windows and doors, in addition to rooms. These are simply represented as two additional semantic categories (on top of the room types).

To represent a floorplan that contains multiple rooms (or floorplan *entities*, such as windows)—each represented as a labeled polygon, as detailed above—we concatenate their sequences using a separator  $\langle \text{SEP} \rangle$  token. We also use  $\langle \text{BOS} \rangle$  and  $\langle \text{EOS} \rangle$  tokens to indicate the beginning and the end of the sequence. Put together, the labeled polygon sequence is structured as follows:

$$[\langle \text{BOS} \rangle, c_1^1, c_2^1, \dots, \langle \text{SEP} \rangle, c_1^n, c_2^n, \dots, \langle \text{EOS} \rangle]$$

As Raster2Seq is trained to regress continuous values without relying on a discrete tokenizer, each token is augmented with a token type probability vector  $q \in [0, 1]^3$ , where the three token type categories are  $\langle \text{CORNER} \rangle$ ,  $\langle \text{SEP} \rangle$  or  $\langle \text{EOS} \rangle$ ; a similar augmentation strategy was recently utilized in [21]. During training, the  $\langle \text{CORNER} \rangle$  type is used as a supervision label for each corner token  $c_i$  but is not explicitly included in the sequence.  $\langle \text{BOS} \rangle$  is omitted from the token type modeling. The training objective is to predict the next corner token in the sequence, where the output sequence contains the target tokens to be predicted; see Figure 2.

### 3.2. Anchor-based Autoregressive Decoder

Next, we present our *Anchor-based Autoregressive Decoder* module which predicts labeled polygon sequences; see Figure 3 for an illustration. Our proposed module is provided with three different inputs: (i) image features extracted with the *Feature Extractor* module, (ii) a sequence of coordinate tokens, and (iii) learnable anchors.

The sequence of coordinate tokens are provided after quantization of the continuous 2D coordinates into a discrete 1D embedding space using a learnable codebook  $C \in \mathbb{R}^{H_b \times W_b \times D}$ , where  $H_b \times W_b$  is number of quantization bins and  $D$  is embedding dimension; additional details are provided in Appendix B. Specifically, the decoder is provided with  $L$  coordinate tokens, which are denoted by  $f_{poly} \in \mathbb{R}^{L \times D}$ . Learnable anchors, denoted by  $v_{anc} \in \mathbb{R}^{L \times 2}$ , are introduced to avoid direct regression of continuous coordinate values. Instead, the model learns residuals relative to these anchors. We demonstrate that the use of learnable anchors yields significant performance gains in Section 4.

**Decoder Architecture.** The decoder contains an autoregressive block that contains three different layers: masked attention, deformable attention, and a feed-forward network layer. In the masked attention layer, a causal mask is applied to ensure that each token can only attend to its preceding tokens, reinforcing a left-to-right generation bias [40]. As shown in Fig. 3, the triplet of query (Q), key (K), and value

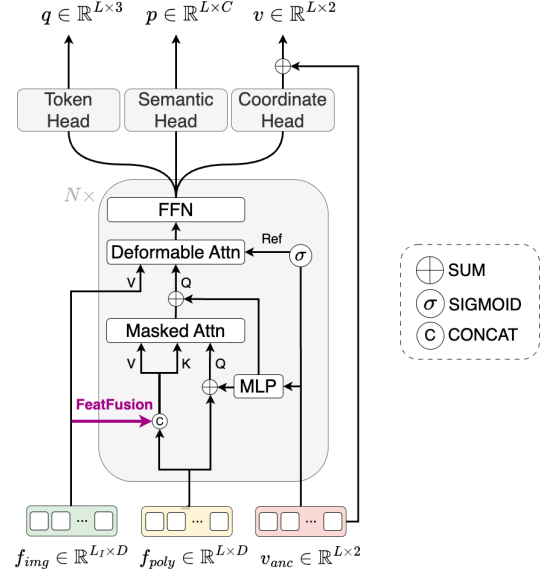


Figure 3. Illustration of our anchor-based autoregressive decoder.

(V) vectors is derived from the sequence of coordinate tokens. The query vector includes additional positional embeddings from the introduced anchors, while the key and value vectors are derived from a fused feature vector of shape  $[L_I + L, D]$ . This fused vector combines image features from the encoder with coordinate-token embeddings through tensor concatenation, referred to as *FeatFusion* (highlighted in purple in Figure 3). We find that this early fusion is crucial for precise coordinate regression. Intuitively, the image features act as a prefix that each token can attend to, providing additional contextual information during decoding.

Subsequently, the output vectors from the preceding masked attention layer serve as queries in a deformable attention module. This module, first introduced in [51], is an efficient attention-based mechanism that—given a feature map and a set of reference points—for each query, only attends to a small set of sampling points around each reference point, rather than the entire feature map. In our autoregressive decoder, this mechanism allows for attending to a sparse set of relevant spatial positions in the image feature map  $f_{img}$ . Specifically, input anchor points are first normalized to  $[0, 1]$  using a sigmoid function. The deformable attention layer then takes in the query vector and predicts offsets relative to these normalized anchor points using a linear layer. These offsets are added to the anchor points to produce sampling points, allowing the attention mechanism to focus on informative regions of image features. As previously mentioned, the anchor points are learnable parameters that are randomly initialized and learned jointly with the network weights.

Finally, the decoder module contains three lightweight heads on top of the last autoregressive block: a token head

for predicting token types, a semantic head for predicting semantic labels, and a coordinate head for predicting 2D corner coordinates. The coordinate head essentially produces residual outputs which are combined with the learnable anchors for producing continuous coordinate values, as illustrated in Figure 3.

### 3.3. Training and Inference Details

Our method is supervised using three different loss functions: a coordinate regression loss, a token-type classification loss, and a semantic classification loss.

**Coordinate loss.** For the coordinate loss, we use a L1 loss to measure the difference between the predicted coordinates  $\hat{v}$  and the ground-truth spatial coordinates  $v$ , across all  $L$  tokens (*i.e.*, corners) in the sequence:

$$\mathcal{L}_{coord} = \frac{1}{L} \sum_{l=1}^L \mathbf{m}_l |\hat{v}_l - v_l|, \quad (1)$$

This loss is computed only over non-padded tokens, using an additional mask  $\mathbf{m}$  to exclude irrelevant positions. The same masking strategy is applied to the other losses described below.

**Token-type loss.** As defined as in Section 3.1, we consider three token classes: <CORNER>, <SEP>, and <EOS>. The model is trained to classify individual token into one of these categories using a standard cross-entropy loss:

$$\mathcal{L}_{token} = \frac{1}{L} \sum_{l=1}^L \mathbf{m}_l \text{CE}(\hat{q}_l, q_l), \quad (2)$$

where  $\hat{q}_l$  is the predicted probability distribution over three token types, and  $q_l$  is the ground-truth one-hot vector for the  $l$ -th token.

**Semantic loss.** We supervise prediction of semantic labels using a cross-entropy loss defined for each token:

$$\mathcal{L}_{sem} = \frac{1}{L} \sum_{l=1}^L \mathbf{m}_l \text{CE}(\hat{p}_l, p_l), \quad (3)$$

where  $\hat{p}_l$  is the predicted probability distribution over  $C$  predefined room classes, and  $p_l$  is the one-hot vector representing the ground-truth room class for the  $l$ -th token in the sequence.

The total training loss is:

$$\mathcal{L} = \lambda_{coord} * \mathcal{L}_{coord} + \lambda_{token} * \mathcal{L}_{token} + \lambda_{sem} * \mathcal{L}_{sem}, \quad (4)$$

where  $\lambda_{coord}$ ,  $\lambda_{token}$  and  $\lambda_{sem}$  are weighting coefficients. To induce strong geometric inductive bias, we perform a left-to-right ordering of the polygon sequence during training,

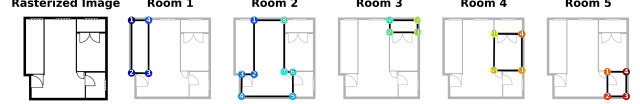


Figure 4. Given an input rasterized image, our method performs sequential corner prediction. We visualize earlier corners in cooler colors (predictions are enumerated per room). As illustrated above, within each room, corners are predicted in counterclockwise order.

where rooms are ordered by top-left coordinates using top-to-bottom, left-to-right scanning priority. As illustrated in our experiments, the model implicitly captures topological relationships between corners, which results in improved performance.

At inference, Raster2Seq predicts tokens sequentially till a <EOS> token is obtained. To predict semantic room labels, we aggregate token-level predictions using a majority voting strategy. Specifically, the room label for each polygon sequence is determined by first selecting the class with the highest probability at each token, and then taking the most frequently predicted class across the sequence. Figure 4 provides a visualization of the sequential room prediction process, illustrating how the model maintains a left-to-right generation pattern. Additional details are provided in the appendix.

## 4. Experiments

In this section, we first describe the experimental setup and the baselines we compare our method against (Section 4.1). We then present our main quantitative results (Section 4.2), followed by both a qualitative comparison (Section 4.3). Finally, we present an ablation study of our proposed method (Section 4.4). Additional details, experiments, ablations, metrics, and a discussion of limitations are provided in the appendix.

### 4.1. Experimental Setup

**Datasets.** We conduct experiments on four datasets: Structured3D [50], Cubicasa5K [17], Raster2Graph [16], and WAFFLE [13]. Structured3D is a 3D point cloud dataset containing 3,000/250/250 training/val/test samples, annotated with 16 room types. CubiCasa5K is a raster-based floorplan dataset with 4,199/399/399 training/validation/test samples, annotated with 11 classes. Raster2Graph has 9,803/500/499 training/validation/test samples, annotated with 12 classes. WAFFLE contains 20K real-world floorplan images scraped from the Internet. As this dataset only contains approximately 100 annotated samples, we only evaluate zero-shot generalization capabilities on this data.

For Structured3D, existing work [47] use the projection of 3D point clouds along the vertical axis as input images. Since our focus is on raster-to-vector floorplan reconstruction, we

Method	Room	Corner	Angle	Room Semantic	Window & Door
<b>Structured3D-B</b>					
HEAT	94.7	84.5	79.6	-	-
PolyRoom	98.9	96.0	91.9	-	-
FRI-Net	96.5	85.4	83.3	-	-
RoomFormer	95.1	91.7	83.2	74.2	94.1
Ours	<b>99.6</b>	<b>98.3</b>	<b>92.7</b>	<b>76.9</b>	<b>98.5</b>
<b>CubiCasa5K</b>					
HEAT	78.2	53.7	32.3	-	-
PolyRoom	54.1	37.1	23.0	-	-
FRI-Net	77.1	50.8	<b>38.0</b>	-	-
RoomFormer	83.5	55.5	34.1	63.0	<b>78.5</b>
Ours	<b>88.7</b>	<b>59.4</b>	37.4	<b>63.8</b>	77.8
<b>Raster2Graph</b>					
HEAT	95.9	79.7	50.9	-	-
PolyRoom	56.9	42.4	23.8	-	-
FRI-Net	91.5	72.3	52.8	-	-
RoomFormer	91.9	74.5	51.1	79.5	-
Raster2Graph	95.0	78.3	<b>67.3</b>	83.4	-
Ours	<b>97.0</b>	<b>80.3</b>	66.6	<b>85.1</b>	-

Table 1. Quantitative comparison on Structured3D-B, CubiCasa5K, and Raster2Graph datasets, evaluating F1 scores across geometric (Room, Corner, Angle) and semantic (Room, Window & Door) predictions. Note that not all models include semantic predictions, and the Raster2Graph dataset does not include Window & Door annotations. Furthermore, the Raster2Graph model can only be evaluated on their dataset, as their approach requires per-corner neighboring room class annotations.

convert the Structured3D samples into binary raster images using the ground-truth annotations, yielding images resembling typical floorplans which are used to train our method. We refer to this converted dataset as Structured3D-B for convenience. Some CubiCasa5K images contain multiple floorplans, so we preprocess them into separate images, increasing the dataset size from 5,000 to 6,281 samples (5,267 train / 503 val / 511 test). We use a fixed resolution of  $256 \times 256$  for all datasets in all experiments.

**Metrics.** We follow the evaluation protocol used by prior work [37], focusing on geometric and semantic metrics obtained from matching model predictions with the ground truth annotations. Three evaluation criteria are Room, Corner, and Angle where each criterion is evaluated using Precision, Recall, and F1 score. Specifically, we first match each ground-truth room with the best-predicted room based on Intersection over Union (IoU), and use these matched pairs to compute evaluation metrics at three levels: room, corner, and angle. For room-level evaluation, a match is considered valid if the IoU exceeds 0.5. For corner and angle evaluation, which are point-wise metrics, we follow the protocol of [37] by computing the L2 distance and the oriented angle between predicted and ground-truth corners. A corner is considered correctly recovered if the distance is within 10 pixels and the angle difference is less than 5 degrees. For semantic label evaluation, room type predictions are additionally used for finding matches. For WAFFLE, we report room

prediction performance using IoU score to access zero-shot performance on the segmentation task. Throughout this section, we mainly use F1 score as the representative measure for Room/Corner/Angle evaluation, additional metrics are reported in the appendix.

**Baselines.** We mainly utilize HEAT [6], RoomFormer [47], FRI-Net [44]—models originally designed for point-cloud density maps—for conducting a quantitative evaluation, fine-tuning these models to perform floorplan reconstruction from rasterized floorplan inputs. We also compare our method against Raster2Graph [16] on raster-to-vector conversion task using their provided dataset. Since Raster2Graph requires per-corner neighboring room class annotations, we can only evaluate it on the Raster2Graph dataset proposed by its authors.

## 4.2. Quantitative Evaluation

We compare performance over the raster-to-vector conversion task across three datasets (see Section 4.1). Overall, our method achieves state-of-the-art performance on both structural metrics (RoomF1 and CornerF1) and semantic metrics (RoomSeemF1 and WindowDoorF1). We note that unlike our method that directly optimizes token-level semantic predictions, RoomFormer dilutes semantic information by averaging irrelevant corners within uniform-length sequences, resulting in inferior semantic predictions as evident across nearly all semantic metrics.

Interestingly, several methods exhibit a high variance in performance across different datasets. In particular, both PolyRoom and FRI-Net achieve very high performance on the simpler Structured3D-B dataset, while achieving significantly lower scores on more complex datasets like CubiCasa5K and Raster2Graph, where polygon lengths are more diverse and shapes are irregular. We hypothesize that PolyRoom’s reliance on segmentation proposals limits its performance to regular and simple floorplans, while FRI-Net’s dependence on line assembly to form rooms proves challenging in diverse scenarios. By contrast, our method achieves strong and stable performance across all three datasets.

**Model Robustness To Floorplan Complexity.** Figure 5 shows the Room F1 performance of RoomFormer, FRI-Net, and our model across varying numbers of polygons and corners on the Structured3D-B and CubiCasa5K datasets. Our method consistently demonstrates greater robustness as floorplan complexity increases. While both models perform similarly on simpler cases, RoomFormer and FRI-Net exhibit a notable performance drop in complex scenes with over 15 polygons or 150 corners. Importantly, RoomFormer operates with a fixed number of room queries (e.g., 2800). Exceeding this capacity causes out-of-memory errors and increased computation due to quadratic attention costs, thus degrading performance on complex floorplans. By contrast,

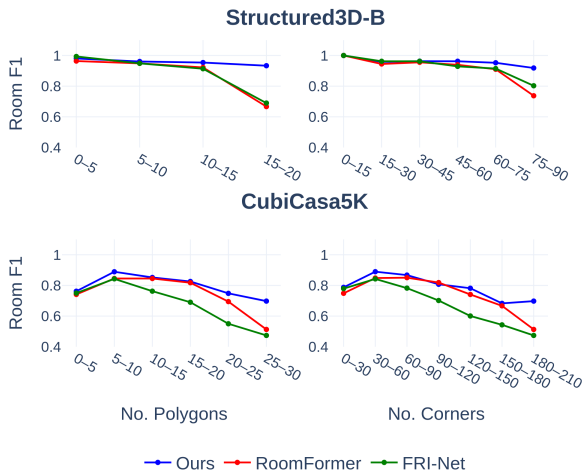


Figure 5. Performance vs. floorplan complexity—as approximated by the total number of polygons (left) and the total number of corners (right). As illustrated above over Structured3D-B (top) and CubiCasa5K (bottom), our approach yields larger gains as the floorplan complexity increases.

our recursive approach decomposes floorplan reconstruction into sub-problems, improving interpretability and naturally handling variable-length inputs.

**Model generalization.** We perform a cross-evaluation experiment across different train-test dataset configuration. We evaluate performance using metrics reported previously, using RoomF1 for the Cubicasa and Raster2Graph dataset and IoU for WAFFLE. Results are reported in Figure 6. As shown, our method demonstrates the strongest generalization performance across various settings, including both same-dataset and cross-dataset evaluations, outperforming other baselines by a large margin. In particular, we observe significant gaps over WAFFLE test set between our method and the counterparts, further demonstrating its robustness on complex and unseen floorplan samples.

**Additional Settings.** In Appendix E.1, we present a quantitative comparison on the standard Structured3D benchmark, using density map inputs rather than rasterized floorplans. As can be observed there, our method achieves competitive results with existing baselines on this additional problem setting. Moreover, we show that our approach is compatible with existing refinement methods [7], which enable additional performance gains.

### 4.3. Qualitative Results

We provide visual comparisons with the RoomFormer model over CubiCasa5K test samples in Fig. 10 and WAFFLE images in Fig. 12. In both cases, the models are trained over the CubiCasa5K train set. These figures illustrate superior visual quality compared to the RoomFormer baseline. In

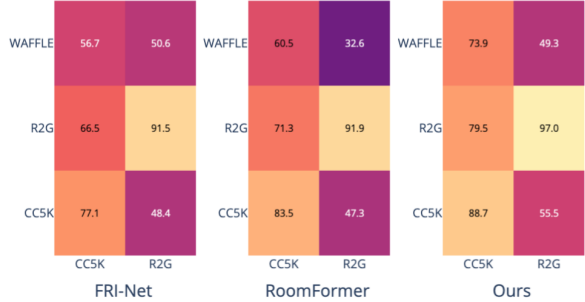


Figure 6. Cross-evaluation heatmaps showing performance across training (rows) and test (columns) dataset combinations, with lighter colors denoting higher performance. R2G and CC5K denote Raster2Graph and CubiCasa5K datasets, respectively. Our method exhibits strong generalization across different settings, substantially outperforming FRI-Net and RoomFormer.

particular, we observe that the RoomFormer model often yields "short-cut" triangular polygons (e.g., leftmost example in Fig. 10), while our model allows for more accurately reconstructing the floorplan's structure.

In Fig. 11, we compare our method with Raster2Graph on their dataset. As clearly seen, our method achieves superior reconstruction quality compared to other counterparts. Notably, Raster2Graph often fails to recover complete floorplan structures, while our approach remains robust across diverse layouts. Note that we only show the structural predictions (without semantics) both here and in the zero-shot generalization experiment over WAFFLE (Fig. 12), as semantic annotations often vary across different datasets. In particular, doors and windows may have different appearances (as illustrated, for instance, by the qualitative results in Fig. 9 and Fig. 10).

**Downstream Application.** Vectorizing rasterized floorplans enables a range of downstream computational tasks that are difficult or impossible to perform directly in pixel space. As a concrete demonstration, we showcase its potential for controllable 3D scene generation. Given a vectorized floorplan, we construct a coarse 3D volume by extruding its boundary geometry along the vertical axis. This volume serves as explicit spatial guidance for a pretrained 3D generative model (*i.e.*, TRELLIS [43]), using the test-time approach introduced in SpaceControl [12]. Figure 7 shows several examples. These results illustrate that floorplan vectorization provides a strong geometric prior, allowing the 3D generative model to faithfully reproduce complex architectural layouts from a single input RGB image, while maintaining global structural consistency.

### 4.4. Ablations

We conduct extensive ablations, evaluating the effect of various components in our framework, on the Structure3D-B

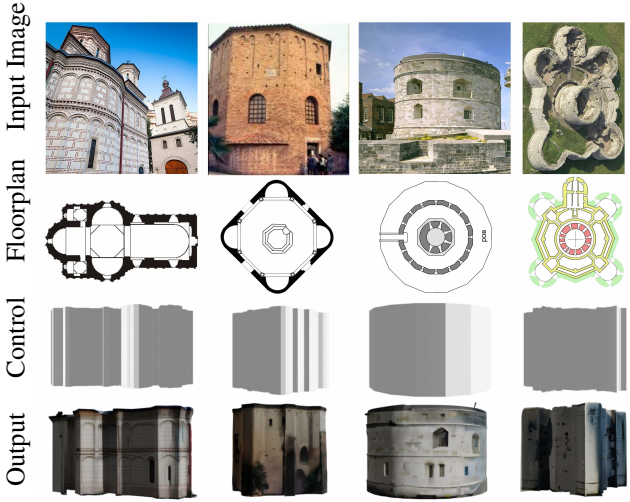


Figure 7. Downstream application: controllable 3D generation from vectorized floorplans. A 3D volume derived from the input floorplan (second row) serves as spatial control (third row) and, together with a conditioning image (top row), guides the generation of 3D scenes (bottom row).

FeatFusion	Anchor	Ordering	Room F1	Corner F1	Angle F1
✓			94.1	91.1	82.0
✓	✓		96.3	93.7	82.6
✓	✓	✓	97.4	95.3	86.0
			99.6	98.3	92.7

Table 2. Ablation studies, evaluating the effect of our *FeatFusion* mechanism, the learnable tokens, and performing a left-to-right ordering of the polygons during training, over the *Structure3D-B* dataset.

dataset. For simplicity of the ablations, we report only the F1 scores for three geometric criteria—Room, Corner, and Angle—with all models trained for 1,350 epochs. As a result, the reported performance in this section does not reflect the best results our model is capable of achieving.

Table 2 highlights the impact of three key components—FeatFusion, which merges polygon and image features, the learnable anchors, and the left-to-right ordering of polygons in the sequence—on floorplan reconstruction performance; qualitative results over a single sample are provided in Figure 8. Incorporating FeatFusion alone yields a notable improvement, *e.g.*, increasing Room F1 from 94.1 to 96.3. Integration of the learnable anchor further boosts performance, with Room F1 reaching 97.4. Further combining the ordering constraint on input training data gives the best overall performance, with a nearly perfect Room F1 and a 6-point improvement for angle metric, illustrating the importance of the left-to-right ordering for effectively training our model. Overall, these results demonstrate the effectiveness of our proposed architectural components.

Additional ablations, quantifying the effect of the se-

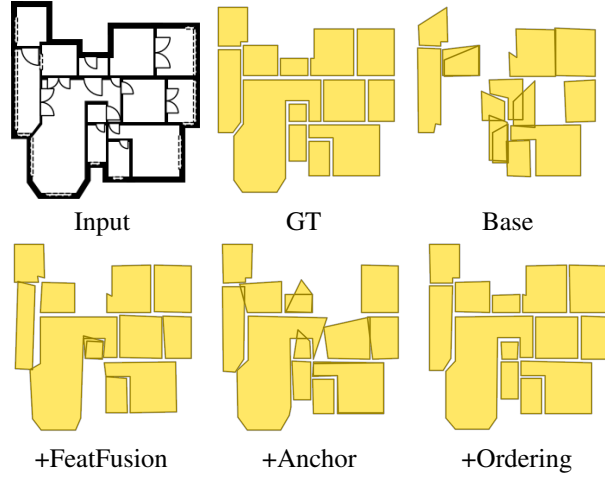


Figure 8. Ablation results over a sample from the *Structure3D-B* test set. As illustrated above, incorporating our proposed components significantly improves geometric reconstruction accuracy and alignment with the groundtruth.

quence length, quantization resolution, and the coefficient of the coordinate loss, are reported in Appendix F.

## 5. Conclusion

In this work, we proposed to frame raster-to-vector floorplan conversion as a sequence-to-sequence task. We introduced a framework that predicts vectorized representation as labeled polygon sequence. The driving mechanism of our framework is an anchor-based autoregressive decoder, that learns to predict the next corner token conditioned on previously generated corners. Technically, our decoder introduces several architectural components, such as the integration of learnable anchors and the *FeatFusion* concatenation operation, enabling for effectively learning the generation of complex polygon sequences. Our experiments demonstrate that our approach outperforms prior work targeting similar tasks across various geometric and semantic metrics.

*Raster2Seq* demonstrates promising generalization performance to *in-the-wild* Internet data, representing a step towards the goal of modeling historical buildings, defined by hand-drawn floorplans. Future work can incorporate mechanisms that further improve results on out-of-distribution data, such as appearance-based augmentations. In particular, combining our system with open-vocabulary predictions could potentially allow for reconstructing the rich semantics reflected in diverse real-world floorplans. More broadly, the ability to recover accurate vectorized floorplan representations will likely become increasingly important as generative models grow more powerful, enabling controllable downstream applications, such as floorplan-guided 3D generation of large architectural scenes, that extend beyond traditional analysis and editing settings.

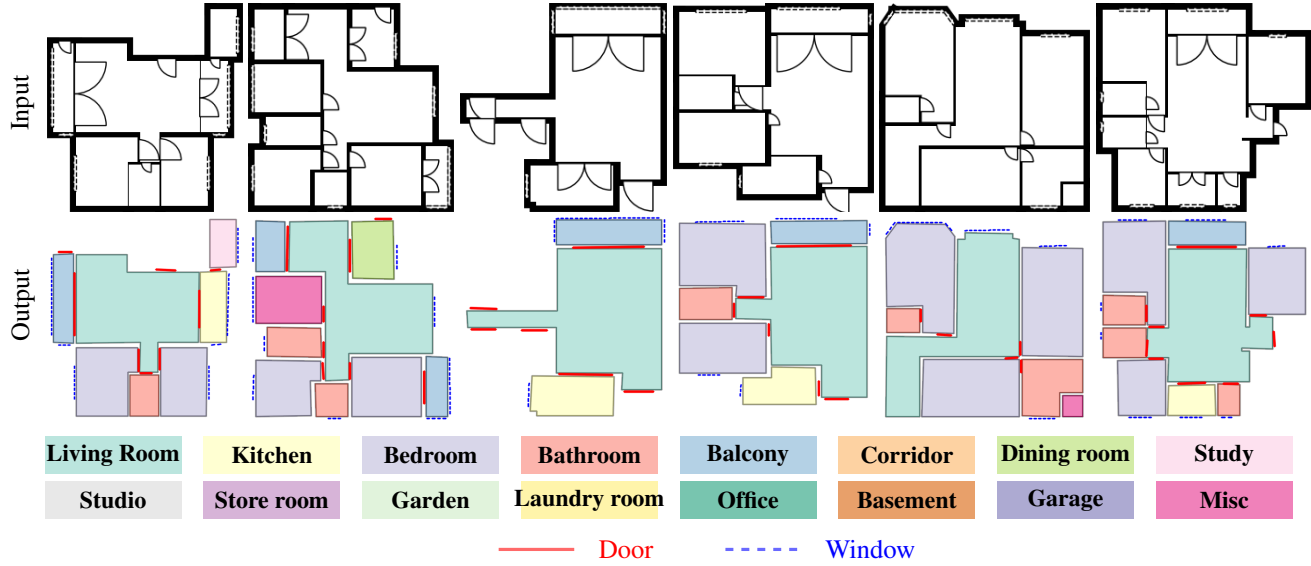


Figure 9. *Raster2Seq* reconstruction results on Structured3D-B.



Figure 10. Qualitative results on the CubiCasa5K dataset, comparing *Raster2Seq* to the *RoomFormer* model.

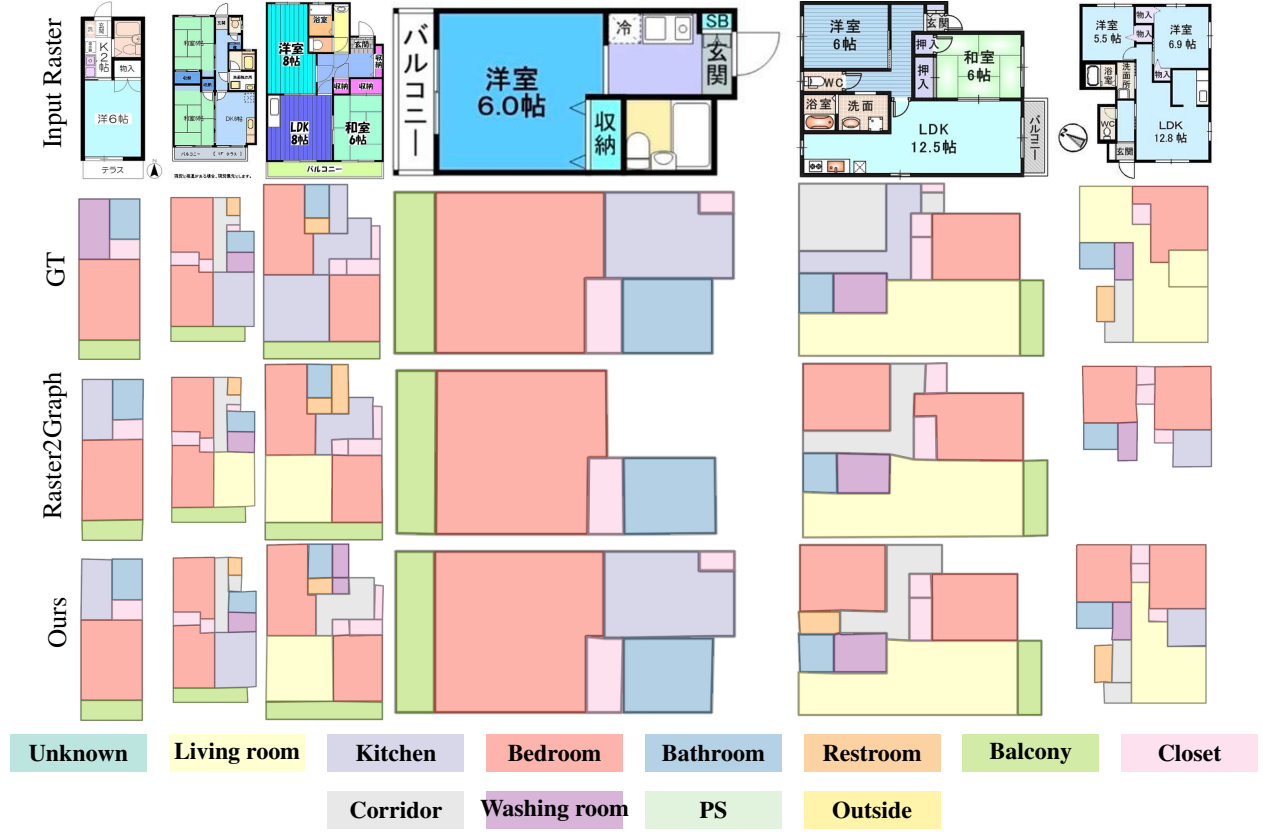


Figure 11. Qualitative comparison with Raster2Graph on their dataset. Our method achieves more accurate floorplan reconstructions in comparison to their model, which often produces incomplete results.



Figure 12. Qualitative comparison with RoomFormer, over WAFFLE floorplan images (both models are trained on CubiCasa5K). As illustrated above, our model exhibits stronger generalization capabilities over the structures of real-world Internet data. Building names from left-to-right: Church of Saint James, the Greater in Rovny, Teltow Canal Power Station, Church of Saint Nicholas, Imkerhaus, Palais du Louvre, Palmer Mansion.

## References

- [1] David Acuna, Huan Ling, Amlan Kar, and Sanja Fidler. Efficient interactive annotation of segmentation datasets with polygon-rnn++. In *Proceedings of the IEEE conference on Computer Vision and Pattern Recognition*, pages 859–868, 2018. 3
- [2] Sheraz Ahmed, Marcus Liwicki, Markus Weber, and Andreas Dengel. Improved automatic analysis of architectural floor plans. In *2011 International conference on document analysis and recognition*, pages 864–869. IEEE, 2011. 2
- [3] Armen Avetisyan, Christopher Xie, Henry Howard-Jenkins, Tsun-Yi Yang, Samir Aroudj, Suvam Patra, Fuyang Zhang, Duncan Frost, Luke Holland, Campbell Orme, et al. Scenescrit: Reconstructing scenes with an autoregressive structured language model. In *European Conference on Computer Vision*, pages 247–263. Springer, 2024. 3
- [4] Ricardo Cabral and Yasutaka Furukawa. Piecewise planar and compact floorplan reconstruction from images. In *2014 IEEE Conference on Computer Vision and Pattern Recognition*, pages 628–635. IEEE, 2014. 2
- [5] Jiacheng Chen, Chen Liu, Jiaye Wu, and Yasutaka Furukawa. Floor-sp: Inverse cad for floorplans by sequential room-wise shortest path. In *Proceedings of the IEEE/CVF International Conference on Computer Vision*, pages 2661–2670, 2019. 2
- [6] Jiacheng Chen, Yiming Qian, and Yasutaka Furukawa. Heat: Holistic edge attention transformer for structured reconstruction. In *Proceedings of the IEEE/CVF conference on computer vision and pattern recognition*, pages 3866–3875, 2022. 2, 3, 6, 18
- [7] Jiacheng Chen, Ruizhi Deng, and Yasutaka Furukawa. Polydiffuse: Polygonal shape reconstruction via guided set diffusion models. *Advances in Neural Information Processing Systems*, 36:1863–1888, 2023. 7, 16, 18
- [8] Ting Chen, Saurabh Saxena, Lala Li, David J Fleet, and Geoffrey Hinton. Pix2seq: A language modeling framework for object detection. *arXiv preprint arXiv:2109.10852*, 2021. 3
- [9] Ting Chen, Saurabh Saxena, Lala Li, Tsung-Yi Lin, David J Fleet, and Geoffrey E Hinton. A unified sequence interface for vision tasks. *Advances in Neural Information Processing Systems*, 35:31333–31346, 2022. 3
- [10] Marcella Cornia, Matteo Stefanini, Lorenzo Baraldi, and Rita Cucchiara. Meshed-memory transformer for image captioning. In *Proceedings of the IEEE/CVF conference on computer vision and pattern recognition*, pages 10578–10587, 2020. 3
- [11] Lluís-Pere De Las Heras, Sheraz Ahmed, Marcus Liwicki, Ernest Valveny, and Gemma Sánchez. Statistical segmentation and structural recognition for floor plan interpretation: Notation invariant structural element recognition. *International Journal on Document Analysis and Recognition (IJ-DAR)*, 17(3):221–237, 2014. 2
- [12] Elisabetta Fedele, Francis Engelmann, Ian Huang, Or Litany, Marc Pollefeys, and Leonidas Guibas. Spacecontrol: Introducing test-time spatial control to 3d generative modeling. *arXiv preprint arXiv:2512.05343*, 2025. 7
- [13] Keren Ganon, Morris Alper, Rachel Mikulinsky, and Hadar Averbuch-Elor. Waffle: Multimodal floorplan understanding in the wild. In *2025 IEEE/CVF Winter Conference on Applications of Computer Vision (WACV)*, pages 1488–1497. IEEE, 2025. 1, 5, 16
- [14] Kaiming He, Xiangyu Zhang, Shaoqing Ren, and Jian Sun. Deep residual learning for image recognition. In *Proceedings of the IEEE conference on computer vision and pattern recognition*, pages 770–778, 2016. 14
- [15] Kaiming He, Georgia Gkioxari, Piotr Dollár, and Ross Girshick. Mask r-cnn. In *Proceedings of the IEEE international conference on computer vision*, 2017. 14
- [16] Sizhe Hu, Wenming Wu, Ruolin Su, Wanni Hou, Liping Zheng, and Benzhu Xu. Raster-to-graph: Floorplan recognition via autoregressive graph prediction with an attention transformer. In *Computer Graphics Forum*, page e15007. Wiley Online Library, 2024. 2, 5, 6, 14, 18
- [17] Ahti Kalervo, Juha Ylioinas, Markus Häkiö, Antti Karhu, and Juho Kannala. Cubicasa5k: A dataset and an improved multi-task model for floorplan image analysis. In *Image Analysis: 21st Scandinavian Conference, SCIA 2019, Norrköping, Sweden, June 11–13, 2019, Proceedings 21*, pages 28–40. Springer, 2019. 1, 5, 14, 17
- [18] Justin Lazarow, Weijian Xu, and Zhuowen Tu. Instance segmentation with mask-supervised polygonal boundary transformers. In *Proceedings of the IEEE/CVF Conference on Computer Vision and Pattern Recognition*, pages 4382–4391, 2022. 18
- [19] Jun Li, Kai Xu, Siddhartha Chaudhuri, Ersin Yumer, Hao Zhang, and Leonidas Guibas. Grass: Generative recursive autoencoders for shape structures. *ACM Transactions on Graphics (TOG)*, 36(4):1–14, 2017. 3
- [20] Manyi Li, Akshay Gadi Patil, Kai Xu, Siddhartha Chaudhuri, Owais Khan, Ariel Shamir, Changhe Tu, Baoquan Chen, Daniel Cohen-Or, and Hao Zhang. Grains: Generative recursive autoencoders for indoor scenes. *ACM Transactions on Graphics (TOG)*, 38(2):1–16, 2019. 3
- [21] Tianhong Li, Yonglong Tian, He Li, Mingyang Deng, and Kaiming He. Autoregressive image generation without vector quantization. *Advances in Neural Information Processing Systems*, 37:56424–56445, 2024. 4
- [22] Chenxi Liu, Alexander G Schwing, Kaustav Kundu, Raquel Urtasun, and Sanja Fidler. Rent3d: Floor-plan priors for monocular layout estimation. In *Proceedings of the IEEE conference on computer vision and pattern recognition*, pages 3413–3421, 2015. 1
- [23] Chen Liu, Jiajun Wu, Pushmeet Kohli, and Yasutaka Furukawa. Raster-to-vector: Revisiting floorplan transformation. In *Proceedings of the IEEE International Conference on Computer Vision*, pages 2195–2203, 2017. 2
- [24] Chen Liu, Jiaye Wu, and Yasutaka Furukawa. Floornet: A unified framework for floorplan reconstruction from 3d scans. In *Proceedings of the European conference on computer vision (ECCV)*, pages 201–217, 2018. 2
- [25] Jiang Liu, Hui Ding, Zhaowei Cai, Yuting Zhang, Ravi Kumar Satzoda, Vijay Mahadevan, and R Manmatha. Polyformer: Referring image segmentation as sequential polygon generation. In *Proceedings of the IEEE/CVF conference on computer vision and pattern recognition*, pages 18653–18663, 2023. 3, 14

- [26] Yuzhou Liu, Lingjie Zhu, Xiaodong Ma, Hanqiao Ye, Xiang Gao, Xianwei Zheng, and Shuhan Shen. PolyRoom: Room-aware Transformer for Floorplan Reconstruction. In *European Conference on Computer Vision*, 2024. 2, 14, 18
- [27] Sébastien Macé, Hervé Locteau, Ernest Valveny, and Salvatore Tabbone. A system to detect rooms in architectural floor plan images. In *Proceedings of the 9th IAPR International Workshop on Document Analysis Systems*, pages 167–174, 2010. 2
- [28] Ricardo Martin-Brualla, Yanling He, Bryan C Russell, and Steven M Seitz. The 3d jigsaw puzzle: Mapping large indoor spaces. In *Computer Vision–ECCV 2014: 13th European Conference, Zurich, Switzerland, September 6–12, 2014, Proceedings, Part III 13*, pages 1–16. Springer, 2014. 1
- [29] Tomáš Mikolov, Martin Karafiat, Lukáš Burget, Jan Černocký, and Sanjeev Khudanpur. Recurrent neural network based language model. In *Interspeech 2010*, pages 1045–1048, 2010. 15
- [30] Medhini Narasimhan, Erik Wijmans, Xinlei Chen, Trevor Darrell, Dhruv Batra, Devi Parikh, and Amanpreet Singh. Seeing the un-scene: Learning amodal semantic maps for room navigation. In *Computer Vision–ECCV 2020: 16th European Conference, Glasgow, UK, August 23–28, 2020, Proceedings, Part XVIII 16*, pages 513–529. Springer, 2020. 1
- [31] Hieu T Nguyen, Yiwen Chen, Vikram Voleti, Varun Jampani, and Huaizu Jiang. Housecrafter: Lifting floorplans to 3d scenes with 2d diffusion model. *arXiv preprint arXiv:2406.20077*, 2024. 1
- [32] Despoina Paschalidou, Amlan Kar, Maria Shugrina, Karsten Kreis, Andreas Geiger, and Sanja Fidler. Atiss: Autoregressive transformers for indoor scene synthesis. *Advances in Neural Information Processing Systems*, 34:12013–12026, 2021. 1
- [33] Akshay Gadi Patil, Omri Ben-Eliezer, Or Perel, and Hadar Averbuch-Elor. Read: Recursive autoencoders for document layout generation. In *Proceedings of the IEEE/CVF Conference on Computer Vision and Pattern Recognition Workshops*, pages 544–545, 2020. 3
- [34] Reiner Pope, Sholto Douglas, Aakanksha Chowdhery, Jacob Devlin, James Bradbury, Jonathan Heek, Kefan Xiao, Shivani Agrawal, and Jeff Dean. Efficiently scaling transformer inference. *Proceedings of Machine Learning and Systems*, 5: 606–624, 2023. 15
- [35] Aditya Ramesh, Mikhail Pavlov, Gabriel Goh, Scott Gray, Chelsea Voss, Alec Radford, Mark Chen, and Ilya Sutskever. Zero-shot text-to-image generation. In *International conference on machine learning*, pages 8821–8831. Pmlr, 2021. 3
- [36] Ka Chun Shum, Hong-Wing Pang, Binh-Son Hua, Duc Thanh Nguyen, and Sai-Kit Yeung. Conditional 360-degree image synthesis for immersive indoor scene decoration. In *Proceedings of the IEEE/CVF International Conference on Computer Vision*, pages 4478–4488, 2023. 1
- [37] Sinisa Stekovic, Mahdi Rad, Friedrich Fraundorfer, and Vincent Lepetit. Montefloor: Extending mcts for reconstructing accurate large-scale floor plans. In *Proceedings of the IEEE/CVF International Conference on Computer Vision*, pages 16034–16043, 2021. 2, 3, 6, 14, 18
- [38] Jiahui Sun, Wenming Wu, Ligang Liu, Wenjie Min, Gaofeng Zhang, and Liping Zheng. Wallplan: synthesizing floorplans by learning to generate wall graphs. *ACM Transactions on Graphics (TOG)*, 41(4):1–14, 2022. 2, 3
- [39] Ilya Sutskever, Oriol Vinyals, and Quoc V Le. Sequence to sequence learning with neural networks. *Advances in neural information processing systems*, 27, 2014. 3
- [40] Ashish Vaswani, Noam Shazeer, Niki Parmar, Jakob Uszkoreit, Llion Jones, Aidan N Gomez, Łukasz Kaiser, and Illia Polosukhin. Attention is all you need. *Advances in neural information processing systems*, 30, 2017. 2, 4, 15
- [41] Oriol Vinyals, Alexander Toshev, Samy Bengio, and Dumitru Erhan. Show and tell: A neural image caption generator. In *Proceedings of the IEEE conference on computer vision and pattern recognition*, pages 3156–3164, 2015. 3
- [42] Shenlong Wang, Sanja Fidler, and Raquel Urtasun. Lost shopping! monocular localization in large indoor spaces. In *Proceedings of the IEEE International Conference on Computer Vision*, pages 2695–2703, 2015. 1
- [43] Jianfeng Xiang, Zelong Lv, Sicheng Xu, Yu Deng, Ruicheng Wang, Bowen Zhang, Dong Chen, Xin Tong, and Jiaolong Yang. Structured 3d latents for scalable and versatile 3d generation. In *Proceedings of the Computer Vision and Pattern Recognition Conference*, pages 21469–21480, 2025. 7
- [44] Honghao Xu, Juzhan Xu, Zeyu Huang, Pengfei Xu, Hui Huang, and Ruizhen Hu. Fri-net: Floorplan reconstruction via room-wise implicit representation. In *ECCV*, 2024. 2, 6, 18
- [45] Kelvin Xu, Jimmy Ba, Ryan Kiros, Kyunghyun Cho, Aaron Courville, Ruslan Salakhudinov, Rich Zemel, and Yoshua Bengio. Show, attend and tell: Neural image caption generation with visual attention. In *International conference on machine learning*, pages 2048–2057. PMLR, 2015. 3
- [46] Jiahui Yu, Yuanzhong Xu, Jing Yu Koh, Thang Luong, Gunnar Baid, Zirui Wang, Vijay Vasudevan, Alexander Ku, Yinfei Yang, Burcu Karagol Ayan, Ben Hutchinson, Wei Han, Zarana Parekh, Xin Li, Han Zhang, Jason Baldridge, and Yonghui Wu. Scaling autoregressive models for content-rich text-to-image generation. *Transactions on Machine Learning Research*, 2022. Featured Certification. 3
- [47] Yuanwen Yue, Theodora Kontogianni, Konrad Schindler, and Francis Engelmann. Connecting the dots: Floorplan reconstruction using two-level queries. In *Proceedings of the IEEE/CVF Conference on Computer Vision and Pattern Recognition*, pages 845–854, 2023. 2, 5, 6, 14, 18
- [48] Zhiliang Zeng, Xianzhi Li, Ying Kin Yu, and Chi-Wing Fu. Deep floor plan recognition using a multi-task network with room-boundary-guided attention. In *Proceedings of the IEEE/CVF International Conference on Computer Vision*, pages 9096–9104, 2019. 2, 3
- [49] Shao-Kui Zhang, Junkai Huang, Liang Yue, Jia-Tong Zhang, Jia-Hong Liu, Yu-Kun Lai, and Song-Hai Zhang. Sceneexpander: Real-time scene synthesis for interactive floor plan editing. In *Proceedings of the 32nd ACM International Conference on Multimedia*, pages 6232–6240, 2024. 1

- [50] Jia Zheng, Junfei Zhang, Jing Li, Rui Tang, Shenghua Gao, and Zihan Zhou. Structured3d: A large photo-realistic dataset for structured 3d modeling. In *Computer Vision–ECCV 2020: 16th European Conference, Glasgow, UK, August 23–28, 2020, Proceedings, Part IX 16*, pages 519–535. Springer, 2020. [5](#), [14](#), [17](#), [18](#)
- [51] Xizhou Zhu, Weijie Su, Lewei Lu, Bin Li, Xiaogang Wang, and Jifeng Dai. Deformable {detr}: Deformable transformers for end-to-end object detection. In *International Conference on Learning Representations*, 2021. [2](#), [4](#), [14](#)

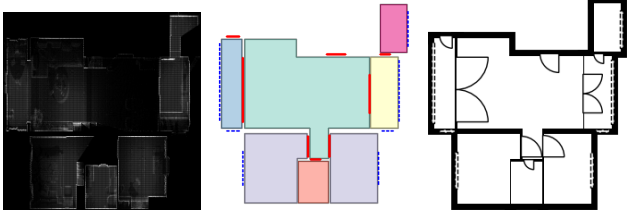


Figure 13. Binary image conversion on Structured3D data. Using the annotated floorplan map, we generate a binary image shown in the last column. Note that the density map on the left is only shown as reference (it is not utilized in the conversion).

In this appendix, we provide additional details on data preparation in Section A. Implementation and training of our method are provided in Section B-C. The algorithm for generating labeled polygon sequences is described in Section D, and additional results are presented in Section E. We also include additional ablations in Section F and provide more qualitative results in Section G. Limitations are discussed in Section H.

## A. Data preparation

### A.1. Structured3D

Since Structured3D [37, 50] is provided as density maps projected from 3D point clouds, we convert these maps into RGB-format floorplan images using the accompanying data annotations (see Fig. 13) to better mimic the appearance of standard RGB floorplans, typically in black-and-white format. Since the raster images in the Structured3D dataset are synthetically generated by a rendering engine, they differ substantially from real-world images in appearance. Meanwhile, the data statistics and annotations after being converted to binary format are preserved without modification.

### A.2. CubiCasa5K

CubiCasa5K [17] is originally proposed for segmentation task where the given annotations are pixel-wise segmentation maps. We first select 10 semantic room classes, namely Outdoor, Wall, Kitchen, Living Room, Bed Room, Bath, Entry, Railing, Storage, Garage, Undefined, along with two additional classes (Window and Door). We convert the segmentation maps of these corresponding classes to polygons which are used as the real-value corners for each room. Since each image may contain more than one floorplan instances, we further process to separate out individual instance which is saved into a separate file (see Fig. 14). Specifically, we take the closed-contours on the binary mask which indicate the foreground/regions of corresponding floorplan instances. After separating out individual instances, we also shift the coordinate of corners based on the bounding box covering floorplan regions.

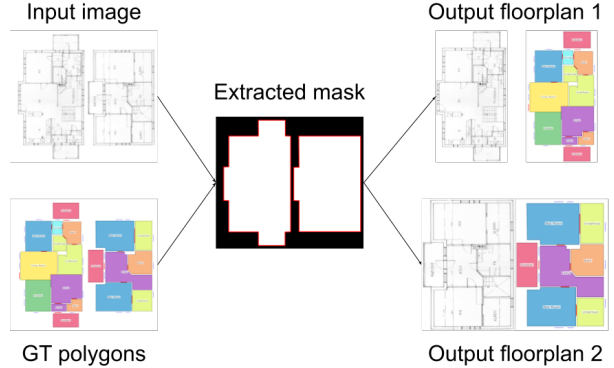


Figure 14. The process of extracting floorplan instances from an image.

### A.3. Raster2Graph

We preprocess the data following Raster2Graph’s codebase [16].

## B. Additional Implementation Details

**Image Feature Extractor.** We instantiate the image feature extractor with a ResNet-50 backbone [14] followed by a transformer encoder [51], following the feature extraction module in [47]. This block produces the feature vector  $f_{img}$  which serves as input to the autoregressive decoder for polygon sequence generation. Followed [16, 26, 47], we initialize the ResNet backbone with ImageNet pretrained weights, then fully finetune the entire network (both backbone and autoregressive decoder) end-to-end.

**Bilinear Quantizer.** In order to train our model on the proposed input sequence, we need to find a suitable way to convert these continuous coordinates to corresponding discrete embeddings. Followed [15, 25], we discritize the 2D contiguous coordinates into 1D embedding space, with an introduction of a learnable codebook of size  $\mathbb{R}^{H_b \times W_b \times D}$  where  $H_b \times W_b$  is number of quantization bins and  $D$  is embedding dimension. In detail, given a 2D coordinate  $(x, y)$ , it is applied floor ( $\lfloor \cdot \rfloor$ ) and celing operations ( $\lceil \cdot \rceil$ ) to produce precise embeddings for its 4 neighbor points in the 2D grid. Formally, the final embedding  $e_{x,y}$  is obtained by a bilinear interpolation to get the exact values of input coordinates:

$$\begin{aligned}
 e_{x,y} = & (\lceil x \rceil - x)(\lceil y \rceil - y) \cdot e_{\lfloor x \rfloor, \lfloor y \rfloor} \\
 & + (x - \lfloor x \rfloor)(\lceil y \rceil - y) \cdot e_{\lceil x \rceil, \lfloor y \rfloor} \\
 & + (\lceil x \rceil - x)(y - \lfloor y \rfloor) \cdot e_{\lfloor x \rfloor, \lceil y \rceil} \\
 & + (x - \lfloor x \rfloor)(y - \lfloor y \rfloor) \cdot e_{\lceil x \rceil, \lceil y \rceil}
 \end{aligned} \tag{5}$$

These quantized values are used as input to the decoder layer, alongside the encoded image features to regress the contiguous coordinate values.

---

**Algorithm 1:** Sequential Corner Generation

---

**Input:** Input image  $I$ , model  $\text{Model}(\cdot)$ , maximum steps  $L_{\max}$

- 1 Initialize sequence  $S \leftarrow []$
- 2 Initialize temporary sequence  $s \leftarrow []$
- 3 Initialize input state  $c_0 \leftarrow [0, 0, p = \emptyset]; q_0 \leftarrow \text{<BOS>}$
- 4 **for**  $l = 1$  **to**  $L_{\max}$  **do**
- // Predict next token
- 5  $\hat{c}_l, \hat{q}_l \leftarrow \text{Model}(I, c_{0:l-1}, q_{0:l-1})$
- 6  $\tilde{q}_l \leftarrow \arg \max(\hat{q}_l)$ ; // Predicted token type
- 7  $\tilde{p}_l \leftarrow \arg \max(\hat{c}_l.p)$ ; // Predicted semantic class
- 8 **if**  $\tilde{q}_l = \text{<EOS>}$  **then**
- 9 **break**
- 10 **if**  $\tilde{q}_l = \text{<SEP>}$  **then**
- 11 Append  $s$  to  $S$ ; // Save current room seq
- 12  $s \leftarrow []$
- 13 **else**
- 14 // Save corner and label
- 15 Append  $[\hat{c}_l.x, \hat{c}_l.y, \tilde{p}_l]$  to  $s$
- 16  $c_l \leftarrow \hat{c}_l; q_l \leftarrow \hat{q}_l$
- 16 **return**  $S$

---

Num bins	Room F1	Corner F1	Angle F1
16x16	95.8	93.4	83.4
32x32	96.3	93.7	82.6
64x64	94.4	91.6	82.8

Table 3. Ablation on coordinate quantization resolution.

Seq length	Room F1	Corner F1	Angle F1
256	92.1	88.0	73.1
512	96.3	93.7	82.6
1024	95.2	92.4	80.0

Table 4. Effect of input sequence length on floorplan generation performance.

**Model configs.** The model consists of 12 layers in total, evenly divided between the encoder and decoder. Since the input sequence length varies across images, we follow standard language modeling practice [29, 40] by padding each input to a fixed length of  $L$  during training.

In the decoder, we introduce a causal attention layer with our proposed post-fusion mechanism, enabling the model to generate outputs autoregressively. This layer is placed before the deformable attention module. The model configuration

	Room F1	Corner F1	Angle F1
In-between (Standard left-to-right)	97.7	95.4	85.1
Post-room (Appending at the end)	98.4	96.4	88.7

Table 5. Ablation on the order of window and doors in the labeled polygon sequence, comparing to a version that treats them like rooms within the standard left-to-right ordering (top) vs. our method which appends them after the room sequence (bottom). This experiment is conducted on Structure3D-B and evaluated at 1749 epoch.

generally follow the former where we keep model dimension at 256 channels. The number of learnable anchors is also set to 512 to match the input length. More details of model configs are shown in Tab. 8.

Additionally, to accelerate the generation, we introduce KV caches [34] for the decoder where the keys and values of previous tokens are stored in the cache, eliminating the cost of recomputing them in every loop.

**Learnable Anchors.** We use learnable anchors for all tokens—both corners and special tokens like  $\text{<SEP>}$  and  $\text{<EOS>}$ —with anchors being fully aware of token types in the sequence. Note that we ignore the coordinate loss for special token positions, which are only supervised by token-type classification, allowing the model to dynamically adjust anchor values based on gradients. At inference, the coordinate values of special tokens are ignored—only their token types are used to identify the end of the current room sequence or the end of generation (see Algorithm 1).

## C. Training details

**Ours.** For training, we also adopt the same hyper-parameters as RoomFormer, detailed in Tab. 7. For pretraining, we train our model for 1400 epochs on Structured3D and 500 epochs on CubiCasa5K. During fine-tuning with semantic loss, we continue training for an additional 450 epochs on Structured3D and 450 epochs on CubiCasa5K. We set  $\lambda_{coord} = 20$  and  $\lambda_{sem} = 1$  by default while  $\lambda_{token}$  is varied for each dataset. All experiments are conducted on a single NVIDIA A6000 GPU and take approximately 1-2 days to complete.

As detailed in the paper (and our ablations), we find that during fine-tuning, the order of coordinates in the sequence matter. Rather than naively inserting window and door coordinates, appending them to the end of the sequence leads to a substantial improvement of model performance. We hypothesize that during pretraining, the model was exposed only to room coordinates. Based on this observation, we append window and door coordinates at the end of the sequence—after the room polygons—to ensure a smooth transition in labeled polygon representation from the pretraining to the finetuning stage (see Tab. 5).

Method	IoU	Prec	Rec
CubiCasa5K pretrained <sup>†</sup>	46.1	79.9	52.1
FRI-Net	56.7	63.4	84.2
RoomFormer	60.5	65.7	88.3
Ours	<b>73.9</b>	<b>81.6</b>	<b>88.6</b>

Table 6. Cross-evaluation of floorplan interior segmentation performance on the *WAFFLE* test set. <sup>†</sup>Reported in [13].

	Structured3D-3DScans	Structured3D-BW	CubiCasa5K	Raster2Graph
Learning rate	2e-4	2e-4	2e-4	2e-4
AdamW optimizer ( $\beta_1, \beta_2$ )	0.9, 0.999	0.9, 0.999	0.9, 0.999	0.9, 0.999
Input image channels	1	3	3	3
Dropout	0.1	0.1	0.1	0.1
Max-grad-norm	0.1	0.1	0.1	0.1
$\lambda_{coord}$	20	20	20	20
$\lambda_{token}$	1	1	5	5
GPUs (A6000)	1	1	1	2
<b>Pretraining</b>				
Epochs	500	1400	500	850
Batch size per GPU	32	32	64	64
Train hours	5.0h	14.3h	19.4h	21.1h
<b>Semantic Finetuning</b>				
Epochs	700	450	450	550
Batch size per GPU	32	32	56	56
Train hours	6.9h	4.6h	16h	13.6h
$\lambda_{sem}$	1	1	1	1

Table 7. Hyper-parameters of pretraining stage.

Config	Value
No. encoder layers	6
No. decoder layers	6
Hidden size	256
FFN hidden size	1024
No. attention heads	8
No. sampling points per deformable attention head	4

Table 8. Model config

**FRI-Net.** The procedure for generating GT occupancy maps for training follows the FRI-Net implementation and no point cloud is needed. These binary maps are generated from GT room polygons (1 for inside, 0 for outside) and used as supervision.

## D. Labeled Polygon Sequence Generation

Algorithm 1 illustrates the corner generation process of our method (inference), which iteratively predicts the next point in the sequence.

## E. Additional Quantitative Results

In this section, we provide a more comprehensive comparison on the Structured3D-B, CubiCasa5K, and Raster2Graph datasets, and the zero-shot setting on the WAFFLE segmentation benchmark. We also report performance on the standard Structured3D density maps. Finally, we present a speed comparison against baselines.

### E.1. Full performance comparison.

Detailed results of Structured3D-B, CubiCasa5K, Raster2Graph are shown in Table 9, Table 10, Table 11, respectively. Overall, we achieve superior geometric performance in two key metrics, Room and Corner, while demonstrating strong semantic floorplan reconstruction results. This is attributed to our labeled polygon representation and our token-wise classification loss.

**Performance on Structured3D Density Maps.** We conduct a comparison on the standard Structured3D benchmark, providing our model with density map inputs for both training and testing. As illustrated in Tab. 12, our method generally outperforms existing baselines on key geometric metrics such as Room and Angle. Although FRI-Net achieves competitive performance with our method when using density maps, performance on image inputs is generally lower (see Tab. 12). We hypothesize that FRI-Net’s reliance on disentangled representations of raw line primitives makes it less robust to the diverse structural and appearance variations present in RGB floorplans compared to the homogeneous nature of density maps. We also report performance using PD [7]—a polygon refinement approach. Our method achieves state-of-the-art performance, demonstrating its compatibility with advanced post-processing techniques.

Regarding semantic metrics, RoomFormer exhibits a significant performance drop of 2–5 points when semantic room types are included. By contrast, our model effectively captures both spatial and semantic attributes without compromising performance. This further demonstrates the efficacy of our polygon representation.

### E.2. Zero-shot performance on unseen WAFFLE.

Table 6 presents the cross-evaluation results for interior segmentation on the WAFFLE test set, using a model trained on CubiCasa5k, without exposure to any WAFFLE samples. Our method achieves the best overall performance, with the highest IoU (73.9), precision (81.6), and recall (88.6). In comparison, RoomFormer falls behind in precision (65.7) and IoU (60.5), indicating less reliable predictions. The pre-trained model, trained for segmentation on the CubiCasa5K dataset, shows the weakest performance—particularly in recall (52.1) and IoU (46.1)—highlighting its limited generalization capabilities. These results demonstrate the superior output quality and generalization ability of our method on complex and unseen floorplan samples.

### E.3. Semantic performance on Structured3D–3D scans

In Tab. 13, we provide the comparison on the semantic scores between ours and RoomFormer on 3D scan inputs. As seen, our method offers superior performance in terms of the room semantic criteria while obtaining slightly lower measures for window and door.

Method	Room			Corner			Angle			Room Semantic			Window & Door		
	Prec.	Rec.	F1	Prec.	Rec.	F1	Prec.	Rec.	F1	Prec.	Rec.	F1	Prec.	Rec.	F1
HEAT	95.3	94.1	94.7	81.8	87.4	84.5	77.0	82.3	79.6	-	-	-	-	-	-
PolyRoom	99.4	98.5	98.9	<b>99.0</b>	93.1	96.0	<b>94.7</b>	89.3	91.9	-	-	-	-	-	-
FRI-Net	97.5	95.4	96.5	88.5	82.6	85.4	86.2	80.5	83.3	-	-	-	-	-	-
RoomFormer	95.8	94.4	95.1	93.0	90.5	91.7	84.4	82.1	83.2	74.7	73.8	74.2	95.0	93.1	94.1
<b>Ours</b>	<b>99.6</b>	<b>99.7</b>	<b>99.6</b>	<u>98.9</u>	<b>97.7</b>	<b>98.3</b>	<u>93.3</u>	<b>92.2</b>	<b>92.7</b>	<b>76.9</b>	<b>76.9</b>	<b>76.9</b>	<b>98.5</b>	<b>98.5</b>	<b>98.5</b>

Table 9. Quantitative evaluation on the *Structured3D-B* test set [50], where the input image is a binary floorplan image (as further detailed in Section 4.1). Best results are in bold.

Method	Room			Corner			Angle			Room Semantic			Window & Door		
	Prec.	Rec.	F1	Prec.	Rec.	F1	Prec.	Rec.	F1	Prec.	Rec.	F1	Prec.	Rec.	F1
HEAT	79.9	76.6	78.2	56.2	51.4	53.7	33.8	31.0	32.3	-	-	-	-	-	-
FRI-Net	82.1	72.7	77.1	<b>69.2</b>	40.1	50.8	<b>51.8</b>	30.0	<b>38.0</b>	-	-	-	-	-	-
RoomFormer	84.7	82.3	83.5	58.1	53.1	55.5	35.7	32.6	34.1	63.8	62.3	63.0	<b>80.8</b>	76.3	<b>78.5</b>
<b>Ours</b>	<b>89.3</b>	<b>88.0</b>	<b>88.7</b>	<u>61.0</u>	<b>57.8</b>	<b>59.4</b>	<u>38.4</u>	<b>36.4</b>	<u>37.4</u>	<b>64.4</b>	<b>63.2</b>	<b>63.8</b>	78.9	<b>76.7</b>	77.8

Table 10. Quantitative evaluation on the *CubiCasa5K* test set [17].

#### E.4. Speed comparison

We report sampling time, training throughput, and training time in Table 14. As seen, our method achieves comparable inference speed to Raster2Graph (0.52s vs. 0.57s) though is slower than the single-pass RoomFormer (0.04s). Despite inference time trade-off, our approach delivers the highest training throughput (63 images/s vs. 24 for RoomFormer and 34 for Raster2Graph), enabling faster training in low-resource settings.

#### F. Additional Ablation Studies

The experiments in this section are primarily conducted on Structured3D-B—the binary dataset—unless explicitly stated otherwise.

**Quantization resolution.** Table 3 presents an ablation study on the effect of coordinate quantization resolution—represented by the number of discretized bins (e.g.,  $16 \times 16$ ,  $32 \times 32$ )—on floorplan reconstruction performance. As shown, a  $32 \times 32$  resolution yields the best overall performance, with the highest Room F1 (96.3) and Corner F1 (93.7), while maintaining competitive Angle F1 (82.6). Both coarser ( $16 \times 16$ ) and finer ( $64 \times 64$ ) quantizations result in reduced performance, suggesting that  $32 \times 32$  offers the best trade-off between granularity and model performance. Given that the input coordinate values lie within the range  $[0, 256]$ , using a fine-grained  $64 \times 64$  quantization may introduce redundant precision and undesirable side effects.

**Random vs. Learnable anchors** As seen in Tab. 15, using random initialized anchors barely bring any improvement compared to the baseline (which does not use anchors). By

jointly training the anchors with model parameters, this give a significant boost to overall measurement, illustrating the importance of *learnable* anchors in our framework.

**Sequence length.** Table 4 examines the impact of input sequence length on floorplan generation performance, comparing sequence lengths ranging from 256 to 1024. The results clearly show that increasing the sequence length significantly improves reconstruction quality across all metrics, with gains of 3–10 points when moving from a length of 256. The highlighted row for length 512 corresponds to the best-performing configuration, indicating that it strikes a sweet spot for capturing structural and geometric details in floorplans effectively.

**Coordinate coefficient.** Table 16 presents an ablation study on the coordinate loss coefficient. In this experiment, we fix the token loss coefficient at 1 to isolate and evaluate the impact of varying the coordinate loss weight. Markedly, setting the coordinate loss coefficient to 20 yields the best overall performance, with Room F1 at 96.3, Corner F1 at 93.7, and Angle F1 at 82.6. Lower (10) and higher (40) values of the coefficient lead to a noticeable drop in all metrics, suggesting that an appropriately balanced coordinate loss is crucial for accurate geometric prediction.

**One-stage training.** In Tab. 17, we find that training the semantic model in one stage achieves comparable scores to the two-stage model (with the same training duration), with negligible decrease in semantic metrics (RoomSemanticF1: 76.9 vs. 76.1). This further demonstrates the flexibility of our model across different training schemes. Here, we opt for a two-stage solution for the optimal performance. Additionally, we conduct an ablation study on generation

Method	Room			Corner			Angle			Room Semantic		
	Prec.	Rec.	F1	Prec.	Rec.	F1	Prec.	Rec.	F1	Prec.	Rec.	F1
HEAT	<b>98.0</b>	93.9	95.9	81.2	78.2	79.7	51.9	49.9	50.9	-	-	-
FRI-Net	94.9	88.4	91.5	<b>86.6</b>	62.1	72.3	63.2	45.3	52.8	-	-	-
RoomFormer	92.0	91.8	91.9	74.8	74.3	74.5	51.2	50.9	51.1	79.6	79.5	79.5
Raster2Graph	97.1	93.0	95.0	79.9	76.8	78.3	<b>68.6</b>	66.0	<b>67.3</b>	85.2	81.7	83.4
<b>Ours</b>	<u>97.2</u>	<b>96.8</b>	<b>97.0</b>	80.4	<b>80.1</b>	<b>80.3</b>	<u>66.7</u>	<b>66.5</b>	<u>66.6</u>	<b>85.3</b>	<b>84.9</b>	<b>85.1</b>

Table 11. Quantitative evaluation on the *Raster2Graph* test set [16].

Method	Room			Corner			Angle		
	Prec.	Rec.	F1	Prec.	Rec.	F1	Prec.	Rec.	F1
MonteFloor [37]	95.6	94.4	95.0	88.5	77.2	82.5	86.3	75.4	80.5
HEAT [6]	96.9	94.0	95.4	81.7	83.2	82.5	77.6	79.0	78.3
PolyRoom [26]	98.9	97.7	98.3	<b>94.6</b>	86.1	<b>90.2</b>	89.3	81.4	85.2
FRI-Net [44]	<b>99.5</b>	<b>98.7</b>	<b>99.1</b>	90.8	84.9	87.8	<b>89.6</b>	<b>84.3</b>	<b>86.9</b>
RoomFormer [47]	97.9	96.9	97.5	89.4	85.5	87.4	83.2	79.7	81.4
RoomFormer (w/ semantic)	95.3(-2.6)	93.5(-3.4)	94.4(-3.1)	85.7(-3.7)	81.8(-3.7)	83.7(-3.7)	78.0(-5.2)	74.5(-5.2)	76.2(-5.2)
<b>Ours</b>	99.0	98.4	98.7	92.0	87.1	89.4	84.7	80.3	82.5
<b>Ours</b> (w/ semantic)	<u>99.1</u>	<u>98.6</u>	<u>98.8</u>	<u>92.1</u>	<b>88.1</b>	<u>90.0</u>	86.1	<u>82.5</u>	84.2
FRI-Net + PD [44]	<b>99.6</b>	98.6	99.1	<b>94.2</b>	88.2	91.1	<b>91.9</b>	86.7	<b>89.2</b>
RoomFormer + PD [7]	98.7	98.1	98.4	92.8	<b>89.3</b>	91.0	90.8	<b>87.4</b>	89.1
Ours + PD	<u>99.4</u>	<b>98.9</b>	<b>99.2</b>	<u>93.2</u>	<u>89.2</u>	<b>91.2</b>	<u>91.0</u>	<u>87.2</u>	89.0

Table 12. Quantitative evaluation on the *Structured3D* test set [50], where the input is a density map generated from top-view projection of the 3D point cloud. In the bottom rows, we report performance using PD [7], a recent refinement method. As illustrated above, our method demonstrates competitive performance on this benchmark, and is compatible with existing refinement methods, which enable further performance gains.

Method	Room Semantic			Window & Door		
	Prec.	Rec.	F1	Prec.	Rec.	F1
RoomFormer	71.5	70.0	70.7	<b>83.4</b>	<b>79.0</b>	<b>81.1</b>
<b>Ours</b>	<b>76.8</b>	<b>76.5</b>	<b>76.7</b>	78.6	77.4	78.0

Table 13. Semantic scores on Structured3D test set [50] where the input image is a point-cloud density map.

Method	Sampling time (bs=1)	Training Throughput (images/s)	Training (Epochs/Time)
HEAT	0.09s	39	400/1.2d
FRI-Net	0.56s	53	1800/3.8d
RoomFormer	0.04s	24	800/7.6d
Raster2Graph	0.57s	34	800/3.1d
Ours	0.52s	63	1400/2.9d

Table 14. Speed comparison. All are computed on a single A6000 GPU. Training time is reported on Raster2Graph dataset.

order, comparing right-to-left versus left-to-right ordering. The flipped version yields similar performance.

**Rasterization loss.** We augmented our method with rasteri-

Anchor	Room F1	Corner F1	Angle F1
Baseline	94.1	91.1	82.0
Random	94.4	90.8	81.4
Learnable	99.6	98.3	92.7

Table 15. Effect of Random and learnable anchors.

Coord. Coeff	Room F1	Corner F1	Angle F1
10	93.2	89.2	74.3
20	96.3	93.7	82.6
40	92.0	87.6	74.0

Table 16. Effect of coordinate loss coefficient on floorplan reconstruction performance.

zation loss [18] as done in RoomFormer (see Tab. 18). On Structured3D-B, CornerF1 and AngleF1 gets an improvement of 0.2 and 1.0, respectively. On CubiCasa5K, the gains are minimal, with CornerF1 improving from 59.4 to 59.8 and

	Room F1	Corner F1	Angle F1	RoomSem F1	WD F1
1stage	99.6	<b>98.4</b>	<b>93.2</b>	76.1	98.4
2stages (vanilla)	99.7	98.3	92.7	<b>76.9</b>	<b>98.5</b>

Table 17. Performance comparison between 2-stages VS 1-stage training where 2-stages training is a vanilla option, including pre-training (no semantic) and finetuning (with semantic). \**RoomSem* and *WD* denote "Room Semantic" and "Window & Door", respectively.

	Room F1	Corner F1	Angle F1
<b>Structured3D-B</b>			
w/o	99.6	98.3	92.7
w/	99.6	<b>98.5</b>	<b>93.7</b>
<b>CubiCasa5K</b>			
w/o	88.7	59.4	37.4
w/	88.7	59.8	37.9

Table 18. Ablation on Rasterization loss.

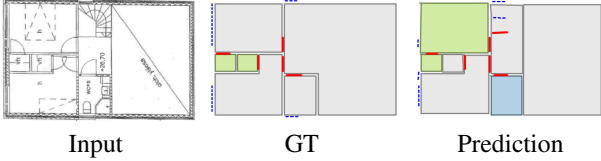


Figure 15. Limitation example, illustrating that our method may generate windows and doors inside rooms. **Red line** denotes a door and a **dashed line** denotes a window.

AngleF1 from 37.4 to 37.9. Since the gain is considerably marginal, we omit this loss for simplicity.

## G. Additional Qualitative Results

Additional qualitative results on Structured3D-B and CubiCasa5K are provided in Fig. 16 and Fig. 17. For more visualization, please refer to our provided interactive tool in additional materials.

## H. Limitations

While our approach achieves strong performance in both geometric reconstruction and generalization, we find that performance over less prevalent semantic structures such as doors and windows can be further refined. As shown in Fig. 15, the model occasionally fails to accurately localize windows and doors, resulting in artifacts such as cross-over windows. Future work can investigate tailored architectural changes to better accommodate other element types, potentially modeling these elements separately from room entities.

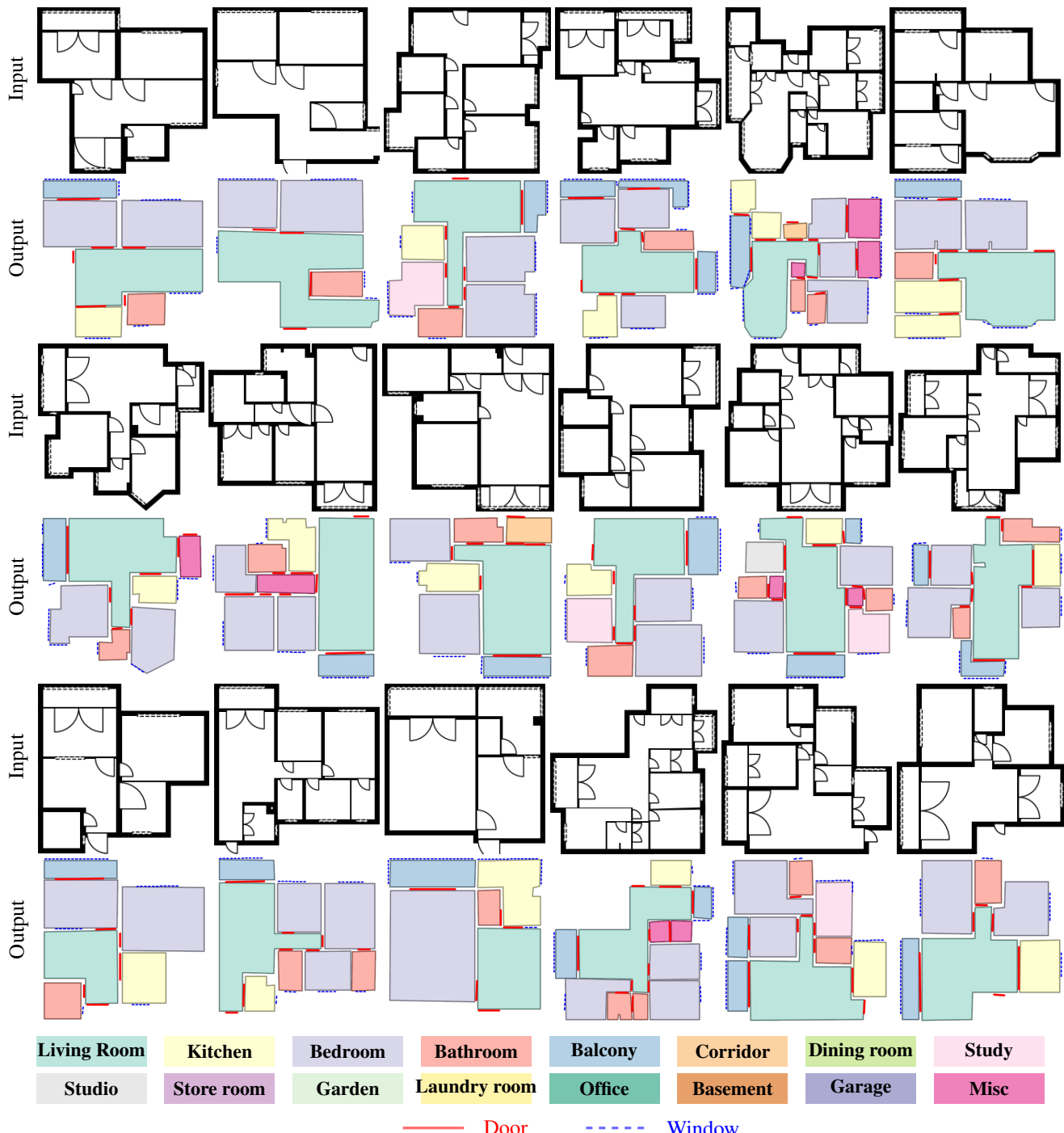


Figure 16. Additional qualitative results on Structured3D.



Figure 17. Additional qualitative results on CubiCasa5K.